Received: 23 January 2020 | Revised: 27 April 2020 | Accepted: 28 April 2020

DOI: 10.1002/mrm.28330

FULL PAPER

Magnetic Resonance in Medicine

3D whole-heart isotropic-resolution motion-compensated joint T_1/T_2 mapping and water/fat imaging

Giorgia Milotta[1] | Aurelien Bustin[1] | Olivier Jaubert[1] | Radhouene Neji[1,2] | Claudia Prieto[1,3] | René M. Botnar[1,3]

[1]School of Biomedical Engineering and Imaging Sciences, King's College London, London, United Kingdom

[2]MR Research Collaborations, Siemens Healthcare Limited, Frimley, United Kingdom

[3]Escuela de Ingeniería, Pontificia Universidad Católica de Chile, Santiago, Chile

Correspondence
Giorgia Milotta, School of Biomedical Engineering and Imaging Sciences, St Thomas' Hospital (3rd Floor-Lambeth Wing), Westminster Bridge Rd, London SE1 7EH, UK.
Email: giorgia.milotta@kcl.ac.uk

Funding information
Grant source: The Engineering and Physical Sciences Research Council (EPSRC); grant numbers: EP/P032311/1, EP/P001009/1, and EP/P007619/1. Grant source: The British Heart Foundation (BHF); grant number: RG/20/1/34802. Grant source: King's College London BHF Centre for Research Excellence; grant number: RE/18/2/34213. Grant source: Wellcome EPSRC Centre for Medical Engineering; grant number: NS/A000049/1. Also, the Department of Health via the National Institute for Health Research (NIHR) Cardiovascular Health Technology Cooperative (HTC) and comprehensive Biomedical Research Centre awarded to Guy's & St Thomas' NHS Foundation Trust in partnership with King's College London and King's College Hospital NHS Foundation Trust

Purpose: To develop a free-breathing isotropic-resolution whole-heart joint T_1 and T_2 mapping sequence with Dixon-encoding that provides coregistered 3D T_1 and T_2 maps and complementary 3D anatomical water and fat images in a single ~9 min scan.

Methods: Four interleaved dual-echo Dixon gradient echo volumes are acquired with a variable density Cartesian trajectory and different preparation pulses: 1) inversion recovery-preparation, 2) and 3) no preparations, and 4) T_2 preparation. Image navigators are acquired to correct each echo for 2D translational respiratory motion; the 8 echoes are jointly reconstructed with a low-rank patch-based reconstruction. A water/fat separation algorithm is used to obtain water and fat images for each acquired volume. T_1 and T_2 maps are generated by matching the signal evolution of the water images to a simulated dictionary. Complementary bright-blood and fat volumes for anatomical visualization are obtained from the T_2-prepared dataset. The proposed sequence was tested in phantom experiments and 10 healthy subjects and compared to standard 2D MOLLI T_1 mapping, 2D balance steady-state free precession T_2 mapping, and 3D T_2-prepared Dixon coronary MR angiography.

Results: High linear correlation was found between T_1 and T_2 quantification with the proposed approach and phantom spin echo measurements ($y = 1.1 \times -11.68$, $R^2 = 0.98$; and $y = 0.85 \times +5.7$, $R^2 = 0.99$). Mean myocardial values of $T_1/T_2 = 1116 \pm 30.5$ ms/45.1 ± 2.38 ms were measured in vivo. Biases of $T_1/T_2 = 101.8$ ms/-0.77 ms were obtained compared to standard 2D techniques.

Conclusion: The proposed joint T_1/T_2 sequence permitted the acquisition of motion-compensated isotropic-resolution 3D T_1 and T_2 maps and complementary coronary MR angiography and fat volumes, showing promising results in terms of T_1 and T_2 quantification and visualization of cardiac anatomy and pericardial fat.

Claudia Prieto and René M. Botnar contributed equally to this work.

KEYWORDS

3D whole-heart, Dixon water/fat separation, respiratory motion correction, T_1 mapping, T_2 mapping

1 | INTRODUCTION

Myocardial tissue characterization plays an important role in the detection of many cardiac diseases.[1,2] Particularly, T_1 mapping has shown promising results in noninvasive detection of cardiomyopathies and diffuse fibrosis,[3-5] whereas T_2 elevation has been correlated with edema associated with myocardial infarction,[6] myocarditis[7] and transplant rejection.[8]

Conventionally, quantitative myocardial T_1 mapping techniques rely on the acquisition of multiple 2D single-shot electrocardiogram-triggered images with variable T_1 contrast. A pixelwise fitting to an exponential model describing the magnetization evolution is performed on the acquired T_1-weighted images to obtain the 2D T_1 maps. Look-Locker–based inversion-recovery sequences sample the longitudinal magnetization recovery curve,[9,10] providing high precision but low accuracy in T_1 quantification. On the other hand, saturation-based recovery acquisitions[11] show better accuracy but lower precision. Both approaches are usually acquired in three 2D short-axis slices in 3 breath-holds, leading to low spatial resolution and limited coverage of the left ventricle. Similarly, conventional cardiac T_2 maps are acquired with a T_2 prepared single-shot balanced steady-state free precession (bSSFP) sequence in 2D short-axis views under several breath-holds. T_2 preparations (T_2prep) with increasing T_2prep duration are used to acquire several T_2-weighted images, and a pixel-wise fitting procedure to an exponential T_2-decay model is then performed to obtain the T_2 map.[12,13] A pause of several heartbeats interrupts the acquisition to allow for T_1 recovery before acquiring the subsequent T_2-weighted image series; thus, only a single 2D slice can be acquired in 1 breath-hold, limiting spatial resolution and coverage.

Recently, 3D free breathing T_1 and T_2 mapping techniques have been proposed to overcome the need for breath-holds, increase spatial resolution, and minimize through-plane motion artifacts.[14-23] Some of these approaches were designed for postcontrast application; thus, a direct extension to precontrast acquisition would not be straightforward.[14,15] Acquisition of 3D free-breathing native T_1 or T_2 maps has been demonstrated using 1D diaphragmatic navigators, but this approach leads to long and unpredictable scan time, limiting spatial resolution and clinical adoption.[14,16,17,19] 1D and 2D self-navigation or fat image navigators enabled the acquisition of 3D T_1 or T_2 maps with 100% respiratory scan efficiency[18,21,24]; however, recovery heart beats for magnetization recovery affect the total scan time, leading to a tradeoff between spatial resolution[18] and acquisition time.[21] A matching approach for T_2 map generation was adopted to avoid the need of pauses for magnetization recovery, enabling the acquisition of high-resolution 3D T_2 maps within a scan time of ~10 min or less,[22,23] relying on 2D image navigators and undersampled acquisition; however, these approaches do not provide T_1 quantification.

The joint acquisition of coregistered T_1 and T_2 maps could improve diagnostic accuracy,[25] avoid misregistration between different acquisitions,[26] and improve efficiency of the acquisition protocol. Several sequences that permit the acquisition of joint myocardial T_1 and T_2 maps in a single scan have been proposed.[27-31] These approaches rely on the combination of magnetization preparation pulses such as inversion recovery (IR), saturation, and T_2prep to achieve combined T_1 and T_2 weighting. Parametric T_1 and T_2 maps are then obtained by fitting the acquired signal to combined relaxometry signal models. However, resting periods are necessary for magnetization recovery, and both 2D breath-held[27,28] and 3D diaphragmatic navigator gated[30] acquisitions suffer from low spatial (anisotropic) resolution and/or limited coverage, hindering the reformatting of the acquired maps in different orientations that could be beneficial for the detection of localized pathologies.

The aim of this work was to develop a novel respiratory motion-compensated whole-heart sequence that provides the acquisition of 3D isotropic resolution joint T_1 and T_2 maps and coregistered anatomical water and fat images from a single free-breathing scan of ~9 min. The proposed approach is based on the acquisition of 4 interleaved volumes with different magnetization preparation pulses and with no interruptions for magnetization recovery. T_1 and T_2 maps are generated by matching the acquired signal evolution to a simulated dictionary. A spoiled gradient echo (GRE) readout with Dixon encoding was used for image acquisition to separate the fat from the water signal to avoid partial volume artefacts and to increase SNR of the water images.[32] Thus, a complementary coregistered 3D T_2-prepared bright-blood water volume for cardiac and coronary anatomy visualization (CMRA) and a fat volume for epicardial and pericardial fat visualization are obtained with the proposed approach. Water/fat cardiac MRI has shown promising results in the assessment of fibro-fatty infiltration in the myocardium and cardiac masses[33,34]; furthermore, it has shown potential in identifying patients with high risk of future cardiac events associated with increased epicardial and pericardial fat.[35] Thus, the proposed technique could enable a comprehensive assessment of cardiac anatomy and tissue characterization.

2 | METHODS

2.1 | 3D Joint T_1/T_2 Framework

The framework of the proposed 3D whole-heart electrocardiogram-triggered joint T_1/T_2 mapping sequence is shown in Figure 1. A similar approach to Ref. 23 was used for the proposed technique; however, an adaptation of preparation pulses and the imaging sequence was crucial to achieve sufficient T_1 and T_2 encoding to provide simultaneous T_1 and T_2 mapping. Four interleaved RF spoiled GRE volumes with 2-point bipolar Dixon encoding were acquired with an undersampled Cartesian trajectory with spiral-like profile order and undersampling factor of 4x.[36,37] The first volume was acquired with a nonselective inversion recovery pulse with TI = 120 ms; the second and third dataset were acquired with no preparations; and a T_2 preparation pulse (T_2prep length = 50 ms) was applied prior to the fourth dataset. A GRE Dixon acquisition was used to obtain a robust water/fat separation independent from the preparation pulses and to increase the SNR of the water images.

2D coronal low-resolution image navigators (iNAVs)[38] were acquired prior to imaging of each volume in order to estimate and correct for superoinferior and left–right respiratory motion, enabling 100% scan efficiency and a predictable scan time. Out-of-phase iNAVs were used to estimate the motion displacements independently for each volume using template matching.[39] This approach ensures that no contrast variations are observed between the iNAVs of each individual dataset. Translational motion correction to a common end-expiration was performed by applying a linear phase shift in k-space[40] to each dataset separately. Finally, a rigid registration to end-expiration is performed between the 4 motion-corrected volumes using mutual information as similarity measure to account for contrast differences. The eight 3D motion-compensated and registered undersampled in- and out-of-phase echoes were jointly reconstructed with a 3D multi-contrast high-dimensionality undersampled patch-based low-rank reconstruction.[41] High-dimensionality undersampled patch-based reconstruction exploits local (within a patch), nonlocal (between similar patches within a neighborhood), and contrast redundancies between the 8 echo images in an efficient multidimensional low-rank formulation. A water/fat separation algorithm with magnitude-based B_0 estimation and phase unwrapping[42] was used to generate the fat and water images for each dataset. The 4 water volumes were normalized on a voxel-by-voxel basis in time to obtain the acquired signal evolution across the 4 acquired volumes. T_1 and T_2 maps were generated by matching the normalized signal evolution of each voxel to a subject-specific simulated dictionary obtained via extended phase graphs (EPG),[43] whereas complementary bright-blood and fat images were obtained from the T_2-prepared dataset. EPG simulations provided the transverse and longitudinal magnetization evolution given a particular sequence design and thus enabled the acquisition of interleaved volumes without need of resting heartbeats for magnetization recovery. Details of dictionary generation and matching step between the acquired and simulated signal evolution are reported hereafter.

2.2 | Dictionary generation and matching

EPG simulations were carried out to generate a subject-specific dictionary. Heart rate-specific parameters such as trigger delay and acquisition window duration were specified for each simulation according to mid-diastolic resting period of the subject acquisition. The MRI signal was simulated at every TR using the EPG framework. Because data acquisition is performed with a centric k-space reordering, the mean absolute value of the transverse magnetization in the central region of the k-space (40%) was considered to generate the dictionary signal evolution. The size of the central region was empirically selected considering the variable density nature of the undersampled trajectory.[36,37] Longitudinal magnetization was used to determine the polarity of the simulated signal. The dictionary was simulated, including variable T_1 and T_2 values in the range [minimum value : step size : maximum value] of T_1 = [60:10:2000] ms and T_2 = [4:2:100, 105:5:200, 210:10:450] ms.[44] Unrealistic T_1 and T_2 pairs, such as those with $T_2 > T_1$, were excluded from the dictionary. The simulated T_1 and T_2 values were selected by considering a wide range of tissues at 1.5 tesla, including healthy myocardium T_1/T_2 = 1090/48 ms[45]; diseased myocardium, that is, fibrosis T_1 = 1300 ms[5,45] and edema T_2 = 60 ms[46]; and blood T_1/T_2 = 1490/240 ms.[45] Matched quantitative T_1 and T_2 maps were generated by minimizing the least square error between the acquired signal evolution and a specific dictionary entry, corresponding to a specific T_1 and T_2 pair, on a voxel-by-voxel basis.

After water/fat separation the signal polarity is lost. To recover the signal polarity before matching, 3 phase-sensitive IR reconstructions[47] were performed between the out-of-phase echoes of 1) IR-prepared and T_2-prepared datasets, and the 2) first and 3) second nonprepared dataset and T_2-prepared dataset, respectively. The 4 motion-corrected water volumes with restored magnetization polarity were then normalized in time by dividing each voxel by the RMS of the corresponding voxel in the 4 volumes.

2.3 | Experiments

The proposed joint T_1/T_2 sequence was tested in EPG simulations, in a T_1/T_2 phantom, and on 10 healthy subjects (4 males, mean age: 31 years, range: 24-37 years). Acquisitions were performed on a 1.5T MR scanner (Magnetom Aera, Siemens

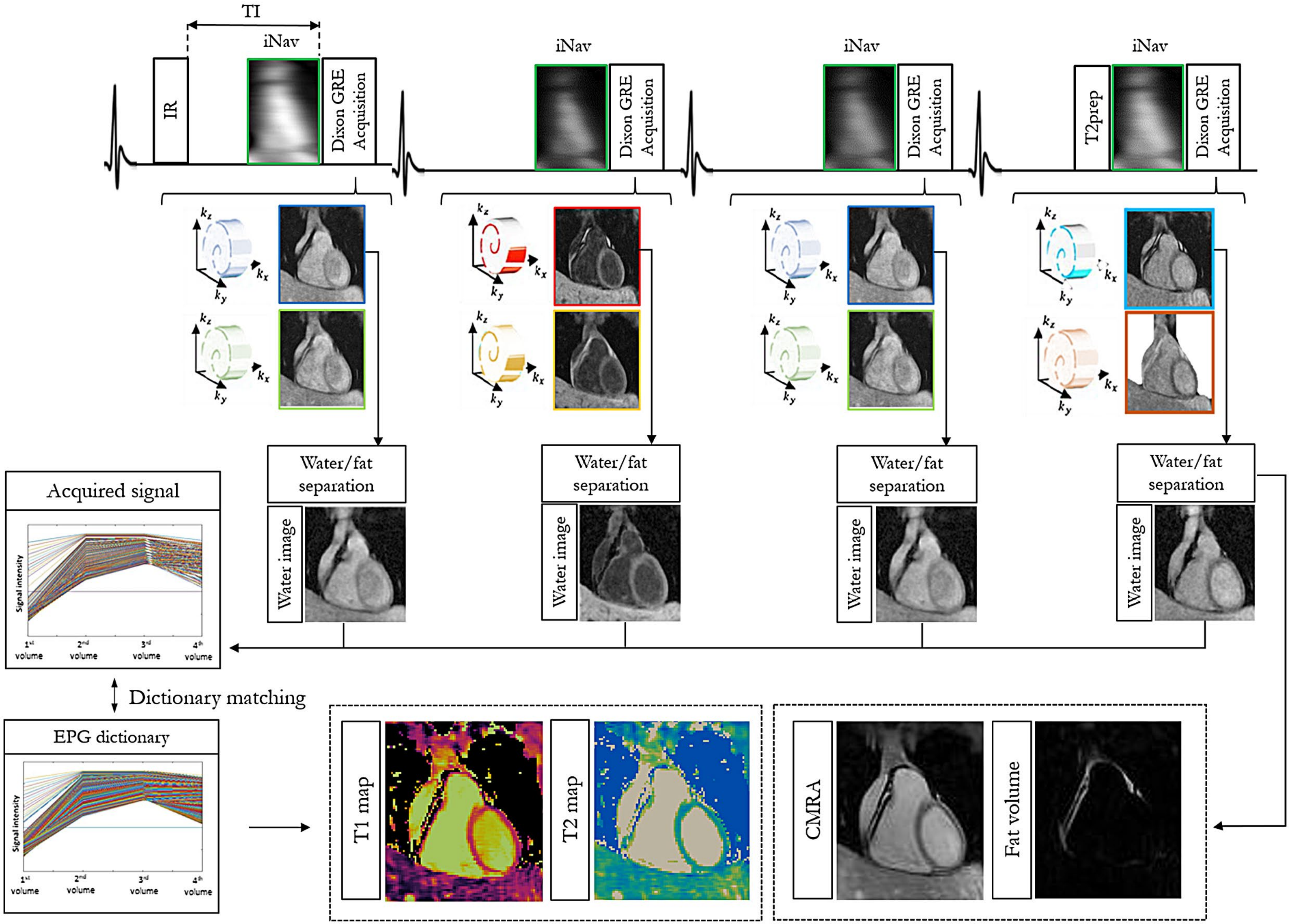

FIGURE 1 Framework of the proposed joint T_1/T_2 mapping sequence. Four interleaved gradient echo volumes with 2-point Dixon encoding and 4x undersampled spiral-like variable density Cartesian trajectory are acquired with different preparation pulses. An IR pulse is performed prior to the first data acquisition; the second and third volumes are acquired with no preparations; and the fourth dataset is acquired with a T_2-preparation pulse. iNAVs are acquired prior to the acquisition to correct for translational respiratory motion. The 8 echoes are motion-corrected to end-expiration and jointly reconstructed with a high-dimensionality undersampled patch-based reconstruction. A water/fat separation algorithm is then used to obtain water and fat images for each acquired volume. T_1 and T_2 maps are generated by matching the acquired signal evolution of the water images to an extended phase graph simulated dictionary. iNAV, image navigator; IR, inversion recovery; TI, inversion time.

Healthcare, Erlangen, Germany) with an 18-channel chest coil and a 32-channel spine coil. Written informed consent was obtained from all participants before undergoing the MR scans, and the study was approved by the institutional review board.

2.3.1 | EPG Simulations

Extended phase graph simulations were used to evaluate the design of the joint T_1/T_2 mapping sequence. EPG dictionaries were generated for 3 different sequence configurations with a reduced number of interleaved volumes (3 to 4) to reduce scan time. The first sequence design included the acquisition of 3 interleaved datasets with (T_I = 120 ms), no-prep, T_2-prep (T_2-prep length = 50 ms) preparations, respectively, and a bSSFP readout with flip angle (FA) = 35 degrees. The second configuration utilized the same preparation pulses, but a GRE readout with FA = 15 degrees was used for imaging. The third sequence configuration included the acquisition of 4 interleaved GRE datasets (IR with TI = 120 ms, no-prep, no-prep, and T_2-prep) with dual echo Dixon encoding (FA = 8 degrees). Landscape graphs[48] comparing the least square error (LSE) between a fixed T_1/T_2 pair and all the other dictionary entries were generated to analyze the T_1 and T_2 encoding provided by the different configurations. The LSE variation around the minimum for a selected T_1/T_2 pair was used as metric for T_1 and T_2 sensitivity of the analyzed sequences. T_1 and T_2 pairs of healthy myocardium ($T_{1\text{healthy-myoc}}$ = 1100 ms, $T_{2\text{heatlhy-myoc}}$ = 50 ms), diseased myocardium ($T_{1\text{diseased-myoc}}$ = 1300 ms, $T_{2\text{diseased-myoc}}$ = 70 ms), and blood ($T_{1\text{blood}}$ = 1400 ms, $T_{2\text{blood}}$ = 250 ms) were investigated.

2.3.2 | Phantom

Data acquisition was performed in a standardized T_1MES phantom[45] to test the sequence accuracy and precision with respect to the phantom reference spin-echo values and conventional 2D MOLLI T_1 mapping and 2D T_2-prepared bSSFP T_2 mapping. The proposed 3D joint T_1/T_2 acquisition parameters included transversal orientation, GRE readout with 2-point Dixon bipolar encoding and centric k-space reordering, FOV = 280 × 280 × 20 mm^3, resolution 2 mm isotropic, TR/TEs = 6.41/2.38/4.76 ms, bandwidth = 485 Hz/pixel, 14 echoes for iNAV acquisition, FA = 8 degrees, TI = 120 ms, T_2prep = 50 ms, 16 segments per heart beat corresponding to an acquisition window of 107 ms, simulated heart rate (HR) of 60 beats per minute (bpm), and acceleration factor of 4 for each acquired volume leading to a total acquisition time of ~2 min. The conventional MOLLI 5(3)3 T_1 mapping sequence was acquired with bSSFP readout, FA = 35 degrees, resolution = 1.6 × 1.6 mm^2, slice thickness = 8 mm, TE/TR = 1.12/2.8 ms, and bandwidth = 1085 Hz/pixel; and 8 single-shot images were acquired with increasing inversion time and 3 recovery heartbeats. The conventional T_2-prepared 2D T_2 mapping imaging parameters included bSSFP acquisition with FA = 70 degrees, resolution = 1.8 × 1.8 mm^2, slice thickness = 8 mm, TE/TR = 1.25/3.5 ms, T_2prep preparations = [0, 28, 55]ms, 3 recovery heartbeats, and linear k-space ordering. Both 2D MOLLI and bSSFP T_2 maps were acquired with a simulated heartbeat = 60 bpm and trigger delay = 700 ms. Three slices were acquired in transversal direction with acquisition time of 11 and 9 heartbeats per slice, respectively.

Additionally, phantom acquisitions with different HRs = [40:20:120] bpm and different acceleration factors (1-4) were performed to investigate the HR and acceleration impact on T_1 and T_2 quantification of the proposed 3D joint T_1/T_2 mapping sequence. The effects of HR variation during a joint T_1/T_2 mapping scan were evaluated by simulating a variable HR ranging between 60 bpm and 100 bpm during an acquisition with a total scan time of 3 min 15 s. The acquired data were matched to a simulated EPG dictionary with fixed HR = 75 bpm.

Another phantom experiment was carried out to evaluate the performance of the water/fat separation algorithm. A standardize T_1MES phantom and a bottle of oil were acquired with the same acquisition parameters as described above.

2.3.3 | Healthy subjects

Data were acquired with the proposed 3D joint T_1/T_2 sequence; conventional 2D MOLLI and 2D bSSFP T_2 mapping; and 3D CMRA sequence with iNAV-based respiratory motion correction and 2-echo Dixon encoding[38] for comparison purposes in terms of T_1/T_2 accuracy, anatomical visualization, and water/fat separation. Imaging parameters for the proposed 3D joint T_1/T_2 sequence included coronal orientation, isotropic resolution = 2 mm, FOV = 320 × 320 × 96−128 mm^3, TI = 120 ms, T_2prep = 50 ms, FA = 8 degrees, TR/TEs = 6.71/2.38/4.76 ms, bandwidth = 485 Hz/pixel, 14 echoes for iNAV acquisition, and acceleration factor of 4x for each volume leading to a total scan time 9 ± 1 min 48 seconds. The 3D CMRA dataset was acquired fully sampled with a single T_2prep of 40 ms and with remaining imaging parameters matching the joint T_1/T_2 acquisition, resulting in a total scan time 16 ± 1 min 34 s. For both 2D MOLLI T_1 mapping and 2D bSSFP T_2 mapping, 3 short axis slices (base, mid, apex) were acquired in 11 and 9 heartbeats breath-holds per slice, respectively, and the imaging parameters matched the phantom acquisition parameters.

A subject-specific trigger delay was selected according to the mid-diastolic resting period for all healthy subject acquisitions.

Trigger delay ranged between 562 to 854 ms, and acquisition window ranged between 94 to 120 ms, corresponding to 14 to 18 segments. The acquisition parameters of the different utilized sequences are summarized in Supporting Information Table S1.

2.4 | Reconstruction

The 2D T_1 and T_2 maps were reconstructed directly on the scanner with inline software (Syngo MR VE11C, Siemens Healthcare, Erlangen, Germany). In-plane motion between the different T_1 and T_2 weighted images was compensated via nonrigid motion correction, and an exponential pixel-wise fitting procedure was performed to obtain the T_1 and T_2 maps. The reconstruction of the 3D T_2-prepared CMRA with Dixon encoding was also performed inline on the scanner. Translational motion correction and iterative SENSE reconstruction were performed for each echo, and water/fat separation was used to obtain the water CMRA and fat volumes.

Joint T_1 and T_2 datasets were reconstructed offline using MatLab R2017a (MathWorks, Natick, MA) on a dedicated workstation (16-core Dual Intel Xeon Processor, 2.3 GHz, 256GB RAM). Translational motion correction to a common end-expiration position was performed for each of the 8 echoes, and was subsequently performed with parameters optimized, as suggested in Ref. 41; in particular patch size $N = 7 \times 7$ and lambda $\lambda = 0.2$ were selected. Finally, a water/fat separation algorithm[42] was used to obtain water and fat images from each dataset. The total reconstruction time to obtain the motion-corrected water and fat volumes was 17 min 36 s. 3D T_1 and T_2 maps were obtained by matching the acquired signal evolution to an EPG-simulated dictionary generated using subject-specific electrocardiogram timestamps, as mentioned before. Total average time to generate a subject-specific dictionary was 6 min 42 s, whereas the averaged matching time to generate T_1 and T_2 maps with a least square minimization was 3 m 28 s.

2.5 | Data-analysis

2.5.1 | Simulations

T_2 sensitivity of a chosen T_1/T_2 pair was quantified as the variation of the LSE for a simulated T_2 variation of ±15 ms from the chosen fixed T_2 value. Similarly, T_1 sensitivity was quantified as LSE variation for a simulated T_1 variation of ±100 ms from the chosen fixed T_1/T_2 value. Higher variation (stronger T_1 or T_2 gradient) indicates a narrower LSE minimum and thus higher sensitivity to the detection of the exact T_1 and T_2 in the presence of noise, guaranteeing a higher accuracy in T_1 and T_2 quantification.

2.5.2 | Phantom

The proposed 3D joint T_1/T_2 and 2D standard T_1 and T_2 mapping sequences were compared in terms of accuracy (bias) and precision (quantified as coefficient of variation [COV]) with respect to phantom reference values by selecting the same region of interest in each phantom vial. Additionally, a Bland Altman analysis was performed to quantify the biases obtained with the proposed approach with respect to conventional 2D sequences. Comparison was also performed for the HR and acceleration factor dependency experiments. The efficacy of water/fat separation was evaluated by measuring the water and fat signal evolutions in each phantom vial and in the oil bottle.

2.5.3 | Healthy subjects

The efficacy of water/fat separation obtained with the proposed approach was qualitatively compared against 3D water CMRA and fat images obtained from the standard 3D T_2-prepared CMRA acquisition with dual-Dixon encoding. Quantitative analysis was performed for T_1 and T_2 values obtained with the proposed approach. Uniformity of T_1 and T_2 quantification was evaluated for 1 representative healthy subject by plotting the per-pixel histogram distribution of T_1 and T_2 quantification throughout the whole left ventricle. Quantitative comparison with standard 2D MOLLI T_1 mapping and 2D bSSFP T_2 mapping was performed by selecting a region of interest in the septum of the myocardium. Mean T_1 and T_2 values and spatial variability were compared for all subjects. Additionally, a Bland Altman analysis was performed to quantify the biases obtained with the proposed approach with respect to conventional techniques. The American Heart Association (AHA) model was used to compare mean T_1 and T_2 values and COV of the proposed 3D joint T_1/T_2 approach and standard 2D T_1 and T_2 mapping techniques. Mean T_1 and T_2 and COV were measured for 16 segments of the AHA model for each healthy subject. The 17th segment was excluded from the analysis due to insufficient coverage of the 2D techniques to image the apical cap.

3 | RESULTS

3.1 | Simulations

The results of the landscape simulations are shown in Supporting Information Figure S1 and Supporting Information Table S2. Similar T_2 LSE variation is observed for all the sequence configurations (~5%, 3%, and 1% for healthy myocardium, diseased myocardium and blood, respectively); thus, comparable accuracy in T_2 quantification is expected among the 3 configurations. On the other hand, the third configuration showed a higher T_1 LSE variation (>2%) for each tissue analyzed compared to configurations 1 and 2; thus, higher accuracy in T_1 quantification and capability to discriminate between healthy and diseased myocardium is expected. The third configuration was therefore chosen as prototype sequence for the proposed method due to better capability of quantifying both T_1 and T_2 values with good accuracy.

3.2 | Phantom

High linear correlations of $y = 1.1 \times -11.68$ ($R^2 = 0.98$) and $y = 0.85 \times +5.7$ ($R^2 = 0.99$) were found between the quantified T_1 and T_2 obtained with the proposed 3D joint T_1/T_2 sequence and spin-echo phantom reference values, respectively, whereas linear correlation of $y = 1.06 \times -33.57$ ($R^2 = 0.98$) and $y = 0.75 \times +17.62$ ($R^2 = 0.92$) were observed between 2D T_1 MOLLI and 2D bSSFP T_2 mapping and phantom reference values, respectively. T_1 and T_2 maps obtained with the proposed 3D technique and 2D conventional mapping approaches, and the measured T_1 and T_2 mean and COV for each phantom vial are shown in Supporting Information Figure S2. The proposed 3D joint T_1/T_2 sequence overestimated the long T_1 = 1489 ms (vial corresponding to blood), whereas an underestimation of long T_2 vials corresponding to blood (T_2s = 189, 243 ms) was observed. This over- and underestimations against reference spin echo sequences led to T_1 and T_2 biases of T_1 = 40.9 ms and T_2 = −8.7 ms, respectively (Figures 2B and 3B); however, a similar trend was observed with the conventional 2D T_1 and T_2 mapping techniques, as shown in Figures 2A and 3A. Biases of T_1 = 31.74 ms and T_2 = −2.4 ms were observed between the proposed technique and the conventional 2D techniques. The variation observed between the proposed sequence and gold standard inversion spin echo and spin echo measurements, excluding the blood vials from analysis, was T_1 = 17.2 ms and T_2 = −2.6 ms. Higher COVs were observed with the proposed technique with respect to conventional 2D MOLLI T_1 mapping for each phantom vial.

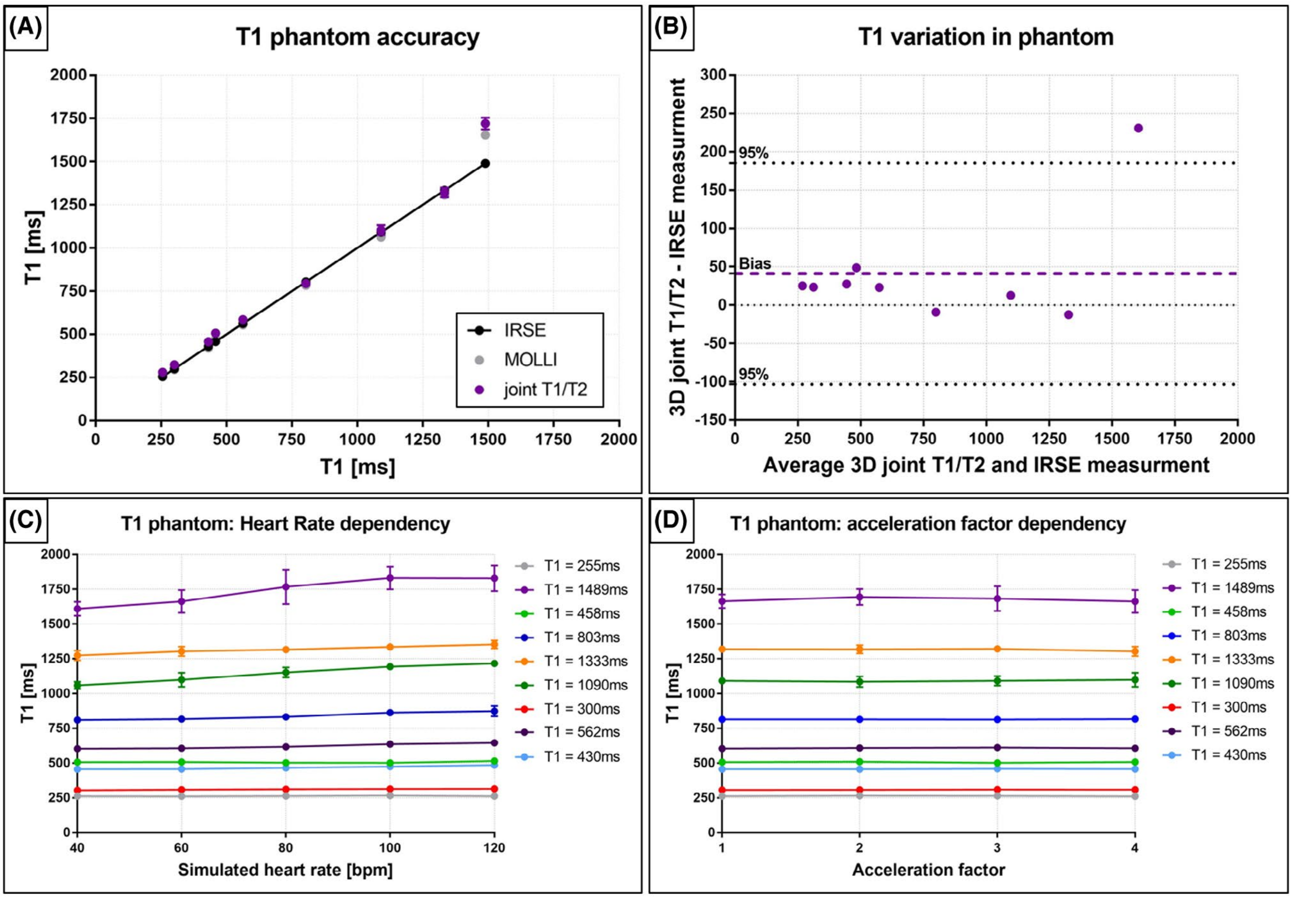

FIGURE 2 T_1 phantom experiments results. (A) accuracy of the proposed technique in comparison to MOLLI and phantom reference IR spin echo values. High linear correlation was found between the proposed approach and the reference values. An overestimation of long T_1 corresponding to blood is observed; similar behavior is obtained with 2D MOLLI acquisition. (B) Bland Altman plot of joint T_1/T_2 sequence and spin echo reference values. A T_1 bias of 40.9 ms was measured. (C) Heart rate dependency of T_1 quantification. A variability of up to 6% was observed for short T_1 values (T_1 < 803 ms), whereas T_1 variability of ~11% was observed for long T_1 values for heart rates ranging between 40 and 120 bpm. (D) T_1 quantification dependency on acceleration factor. A variability of <3% was observed for each phantom vial. bpm, beats per minute; IRSE, inversion spin echo

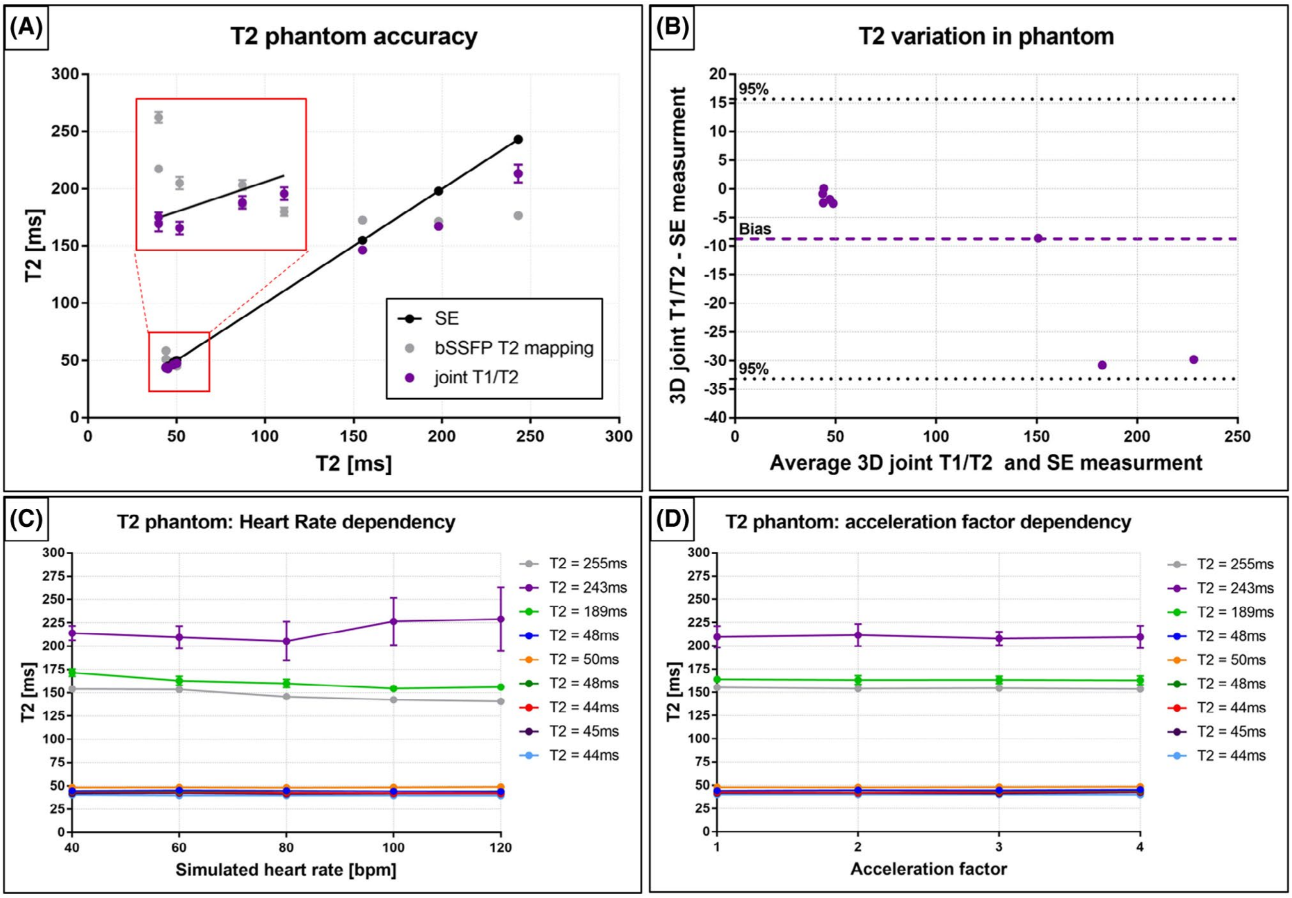

FIGURE 3 T_2 phantom experiments results. (A) Accuracy of the proposed technique in comparison to T_2-prepared bSSFP T_2 maps and phantom reference spin echo values. High linear correlation was found between the proposed approach and the reference values. An underestimation of long T_2 corresponding to blood is observed; similar results are obtained with the 2D bSSFP T_2 mapping approach. (B) Bland Altman plots of joint T_1/T_2 sequence and spin echo reference values. A T_2 bias of −8.7 ms was measured. (C) Heart rate dependency of T_2 quantification. A small variability (<4%) was observed for short T_2 values; T_2 variability of up to 9% was measured for T_2 values corresponding to blood for heart rate ranges of 40 to 120 bpm. (D) T_1 quantification dependency on acceleration factor. A variability of <2% was observed for each phantom vial. bSSFP, balanced steady-state free precession; SE, spin echo

Similar COV was observed for T_2 with the proposed technique and conventional T_2prepared bSSFP T_2 mapping; however, lower precision was obtained with the proposed method for the vial corresponding to blood (Supporting Information Figure S2).

The effect of HR variability on T_1 and T_2 quantification are shown in Figures 2C and 3C, respectively. A variability of <6% was observed for short T_1s (T_1 range = 255-803 ms) for HR ranging between 40 to 120 bpm, whereas a higher variability of ~11% was obtained for long T_1s between 1090 ms and 1489 ms. Similar results are obtained for T_2 quantification, with a variability of <4% being observed for short T_2s corresponding to myocardium T_2 values, whereas variabilities between 6% and 9% were observed for long T_2s corresponding to blood. The effects of HR variability during a scan on T_1 and T_2 estimation are shown in Supporting Information Figure S3. A linear correlation of $y = 0.90 \times +62.4$ (R^2 = 0.99) and a bias = −12.44 ms were found between the T_1 quantified with the proposed sequence and inversion spin echo measurements. Similarly, a linear correlation of $y = 0.92 \times +9.4$ ($R^2 = 0.95$) and bias = 1.5 ms were observed between the T_2 quantified with the proposed sequence and the spin echo reference. In addition, acceleration factor variability was similar for all phantom vials, with T_1 and T_2 variations found to be ~3% for acceleration factors ranging between 1 and 4 (Figures 2D and 3D). Finally, a consistent water/fat separation was observed for each acquired contrast, with a maximum fat signal measured in the water IR-prepared dataset of 1.9 ± 0.4 e−07 (Supporting Information Figure S4).

3.3 | Healthy subjects

Coregistered bright-blood CMRA dataset, fat volume, and T_1 and T_2 maps reformatted in 2-chamber, 4-chamber, and short axis orientation are shown in Figure 4 for 1 representative healthy subject. Water/fat separation was achieved for the entire 3D volume with good delineation of anatomical

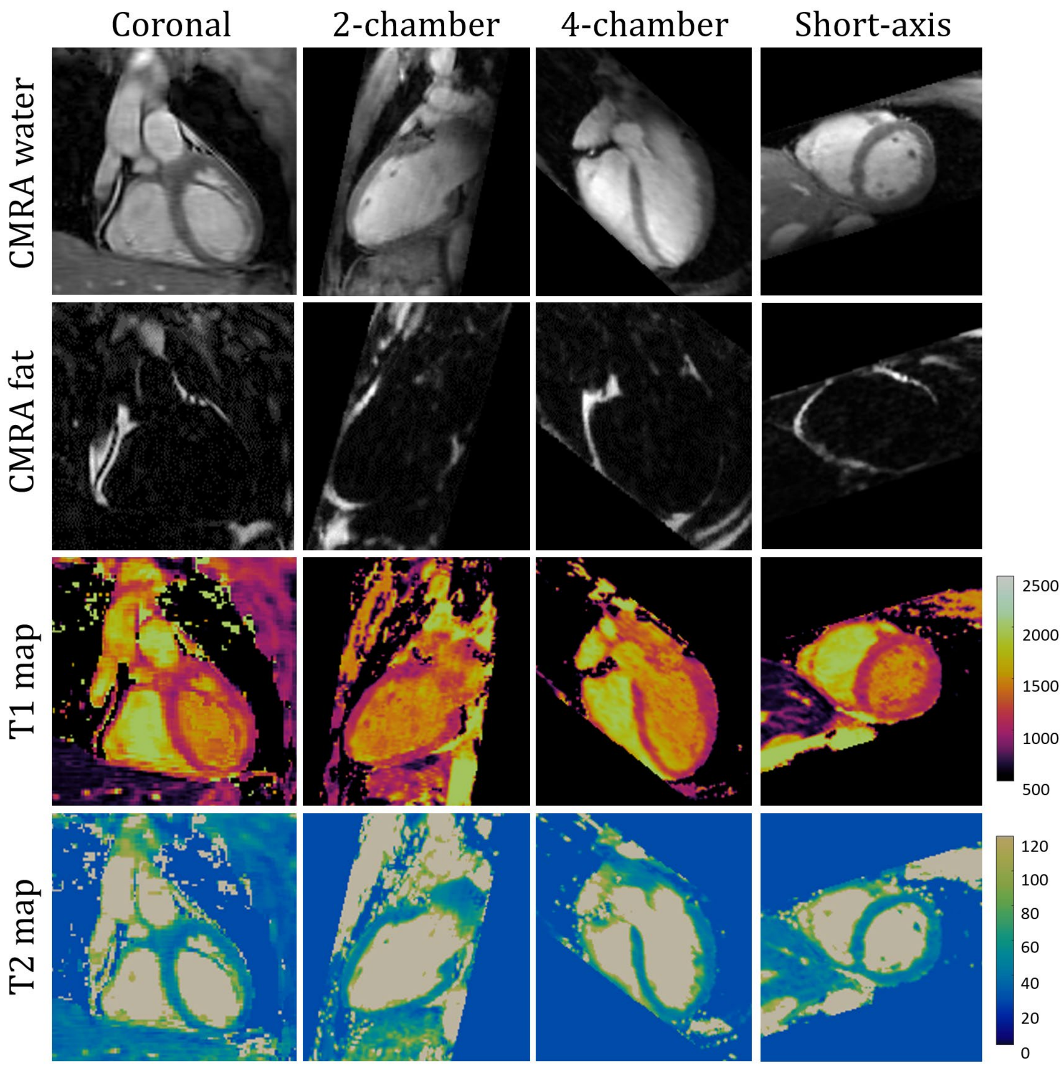

FIGURE 4 Coregistered 3D bright-blood dataset (T_2-prepared), fat volume, and T_1 and T_2 maps obtained with the proposed approach and reformatted in different orientations (coronal, 2-chamber, 4-chamber, and short-axis) for 1 representative healthy subject. Good depiction of cardiac structure such as right coronary artery and papillary muscles is achieved in the bright-blood dataset. Good water/fat separation is obtained across the whole 3D volume, and uniform T_1 and T_2 quantification are shown in the different orientations

structures, such as the right coronary artery and papillary muscle, obtained in the water CMRA dataset. The coregistered T_1 and T_2 maps showed good delineation of the left ventricle with uniform quantification of T_1 and T_2 values. Efficacy of the water/fat separation algorithm for each acquired 3D volume is shown in Figure 5 and compared with a T_2-prepared (T_2prep = 40 ms) 2-echo Dixon CMRA. Comparable water/fat separation was observed for the second, third, and fourth dataset of the joint T_1/T_2 mapping sequence and the standard T_2-prepared CMRA acquisition, with no observable water/fat swaps in the cardiac region for each reconstructed dataset. A fat underestimation was observed in the IR-prepared dataset acquired with the joint T_1/T_2 sequence due to a partial fat suppression effect generated by the nonselective short-TI inversion recovery pulse.[49] T_1 and T_2 maps reconstructed with and without fat/water separation are shown for 1 representative healthy subject in Supporting Information Figure S5. Pericardial fat is clearly visible in the T_1 and T_2 maps reconstructed without water/fat separation. T_1 and T_2 values measured in the myocardial septum of the volumes obtained without water/fat separation were $T_{1no\_W/F} = 1138 \pm 151$ ms and $T_{2no\_W/F} = 43 \pm 7.2$ ms, respectively, whereas a $T_{1W/F} = 1076 \pm 62$ ms and $T_{2W/F} = 45 \pm 2.6$ ms were measured when using the complete proposed framework.

Uniformity of T_1 and T_2 quantification obtained with the proposed joint T_1/T_2 sequence was evaluated for 1 representative healthy subject (Figures 6 and 7). Sixteen coregistered short axis views are shown for both T_1 and T_2 maps, enabling complete coverage of the left ventricle. Mean T_1 values of 1073 ms with SD of 102 ms was measured throughout the whole left ventricle in the per pixel-histogram representation. The AHA 17-segment T_1 bull's eye plot showed uniform T_1 quantification, with slight underestimation in the lateroanterior region of the heart. T_2 per-pixel histogram quantified a

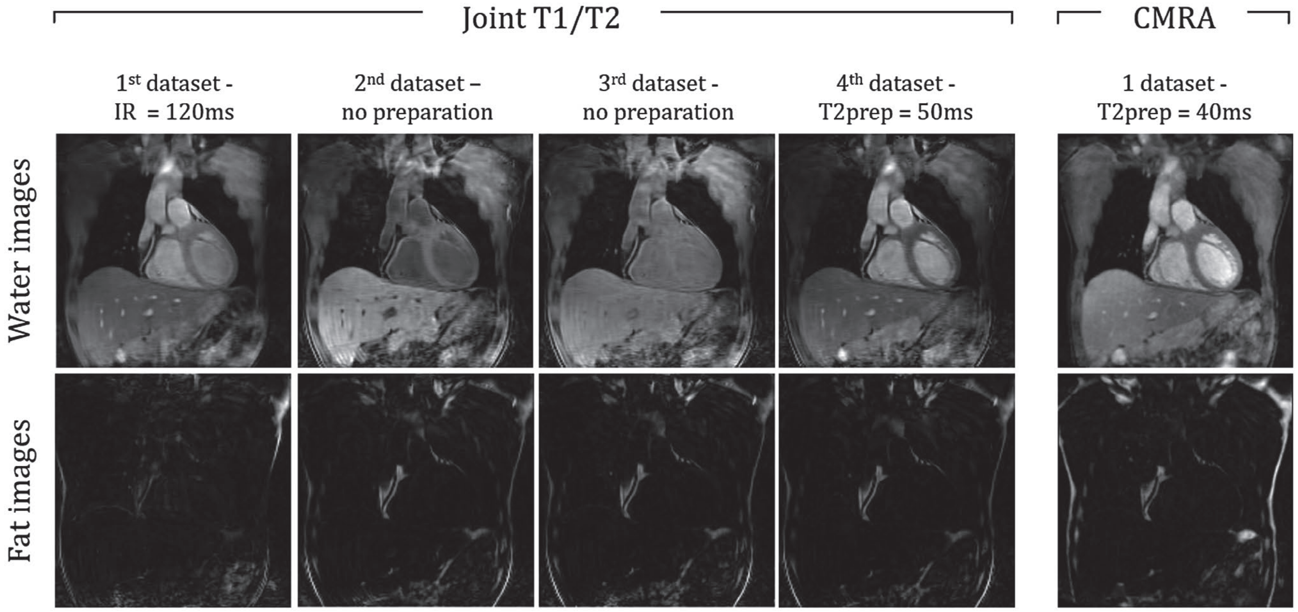

FIGURE 5 Comparison between the offline water/fat separation obtained with the proposed approach for each acquired volume and a 3D CMRA acquired with dual-echo Dixon encoding, iNAVs for motion correction, and inline reconstruction implemented on scanner software. Good water/fat separation is obtained across the whole 3D volume, with comparable results to standard 3D CMRA acquisition. A lower fat signal is obtained from the first volume because the IR preparation pulse acts as a short IR fat suppression pulse, thereby compromising the performance of Dixon water/fat separation. CMRA, coronary magnetic resonance angiography

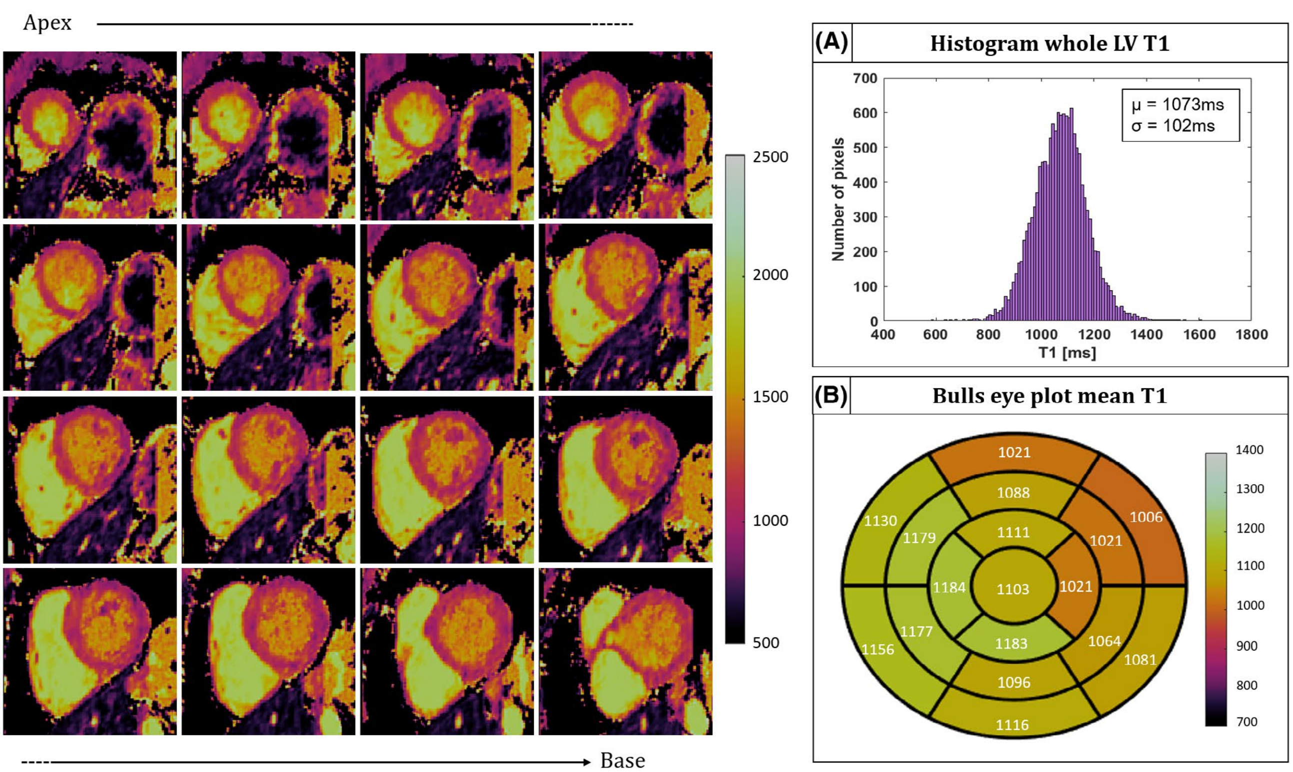

FIGURE 6 T_1 map short-axis views from the apex to the base of the LV for 1 representative healthy subject. Whole LV coverage is obtained with the proposed approach. (A) Per-pixel histogram distribution of measured T_1 values. A mean T_1 value of 1073 ms was obtained with a spatial variability of 102 ms. (B) AHA 17-segment model of T_1 distribution. A lower T_1 was measured in the lateroanterior portion of the LV. AHA, American Heart Association; LV, left ventricle

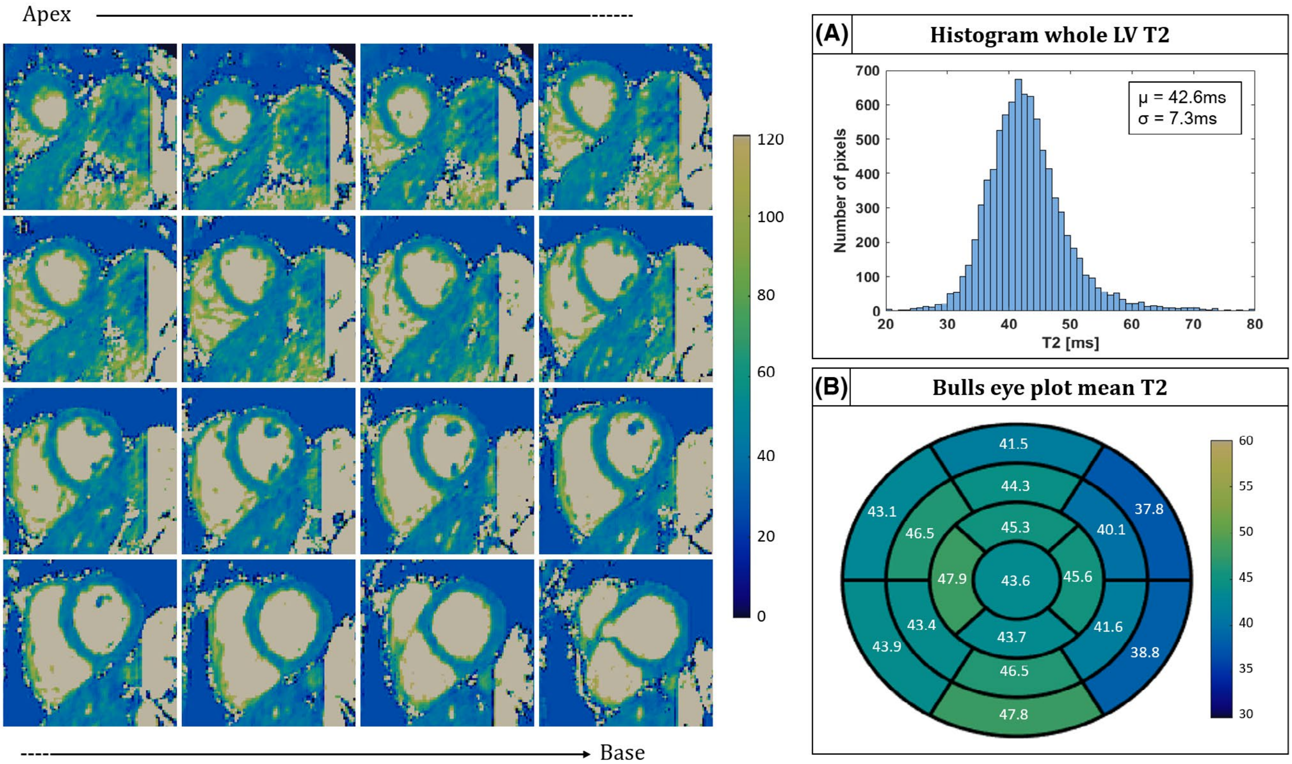

FIGURE 7 T_2 map short-axis views from the apex to the base of the LV for 1 representative healthy subject. Whole LV coverage is obtained with the proposed approach. T_2 maps are coregistered with the T_1 maps shown in Figure 6. (A) Per-pixel histogram distribution of measured T_2 values. A mean T_2 value of 42.6 ms was obtained with a spatial variability of 7.3 ms. (B) AHA 17-segment model of T_2 distribution. A lower T_2 was measure in the lateral portion of the LV

mean T_2 value of 42.6 ms with SD of 7.3 ms; T_2 bull's eye plot showed uniform quantification throughout the 17 segments with T_2 underestimation in the lateral area of the left ventricle.

The mean T_1 and T_2 distributions throughout the left ventricle averaged across all the acquired healthy subjects are shown in a bull's eye plot representation in Supporting Information Figure S6A and B. Additionally, the box plots for all AHA segments are shown in Supporting Information Figure S6C and D for T_1 and T_2, respectively. A slightly higher T_1 (not significant) and T_2 ($P < .05$) values were observed at the apex of the left ventricle (mean $T_{1apex} = 1130 \pm 43$ ms, mean $T_{2apex} = 47.3 \pm 0.9$ ms) with respect to mid- and basal slices (mean $T_{1mid} = 1108 \pm 44$ ms, mean $T_{2mid} = 46.9 \pm 1.2$ ms, mean $T_{1base} = 1116 \pm 19$ ms, mean $T_{2base} = 45.5 \pm 1.2$ ms). Additionally, a statistically significant ($P < .005$) decrease in T_1 was observed from the septal to the lateral region of the left ventricle (mean $T_{1septal} = 1152 \pm 22$ ms, mean $T_{1lateral} = 1084 \pm 26$ ms), whereas a slight, nonsignificant, T_2 decrease from the septum $T_{2septum} = 46.7 \pm 1.4$ ms to the lateral wall $T_{2lateral} = 45.1 \pm 1.1$ ms was observed.

The proposed joint T_1/T_2 sequence was compared to standard T_1 MOLLI and T_2 bSSFP technique. A qualitative comparison between 2D MOLLI T_1 maps, 2D bSSFP T_2maps, and 3D joint T_1/T_2 maps are shown in Figure 8 for 4 representative healthy subjects. Good agreement in depiction of the left ventricle was obtained between the proposed technique and the conventional 2D mapping techniques. A higher mean T_1 value was obtained with the proposed approach compared to MOLLI, whereas comparable T_2 values were observed with respect to T_2-prepared bSSFP acquisition. Higher spatial variability was observed for both T_1 and T_2 maps acquired with the proposed approach; however, by reconstructing the 3D maps to the same slice thickness of the conventional 2D maps, an increased uniformity in T_1 and T_2 quantification is obtained. These qualitative results are confirmed by the quantitative results shown in Figure 9 for T_1 and in Figure 10 for T_2 for each acquired subject. Mean T_1 values and SD in the septum obtained with the proposed approach and MOLLI were respectively $T_{1jointT1/T2} = 1116 \pm 31$ ms and $T_{1MOLLI} = 1014 \pm 32$ ms. A T_1 overestimation in the septum with respect to the 2D MOLLI sequence was observed, with the proposed approach leading to a bias of $T_1 = 101.8$ ms (Figure 9A,C). Good agreement in T_2 quantification was found between the 3D joint T_1/T_2 mapping acquisition and 2D bSSFP T_2 maps in the septum of the left ventricle ($T_{1jointT1/T2} = 45.1 \pm 2.4$ ms and $T_{1bSSFP} = 45.9 \pm 2.2$ ms), with a small bias of $T_2 = -0.77$ ms (Figure 10A,C). A statistically significant higher spatial variability was obtained

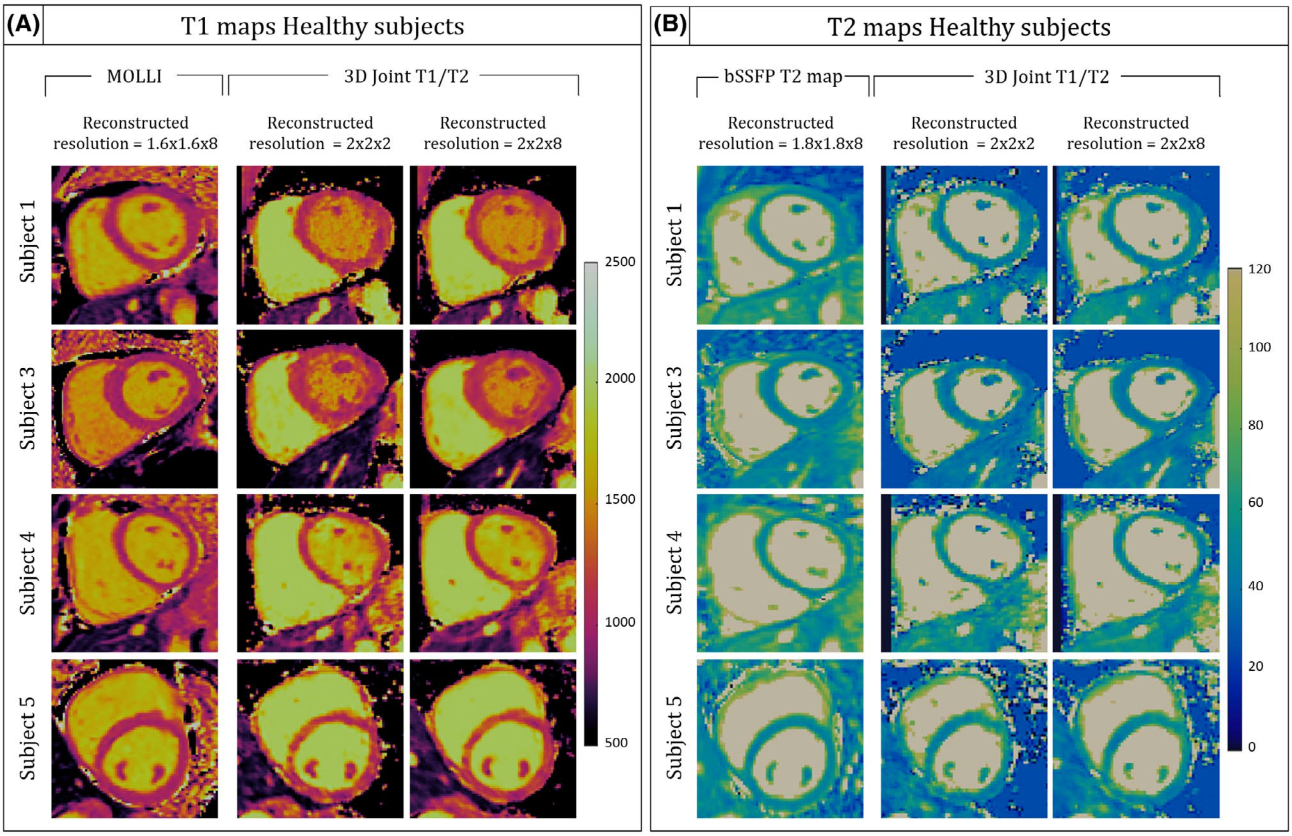

FIGURE 8 Qualitative comparison between T_1 and T_2 maps obtained with the proposed 3D joint T_1/T_2 sequence and standard 2D clinical acquisition for 4 healthy subjects. The acquired 3D T_1 and T_2 maps were reformatted to the same slice position as the 2D maps acquired in short axis. (A) T_1 results: Good depiction of the LV is obtained with the proposed approach, with similar image quality with respect to 2D MOLLI acquisition. A higher T_1 value and higher spatial variability is observed with the 3D joint T_1/T_2 sequence. Spatial variability appears reduced by reconstructing the T_1 maps to same slice thickness as for the 2D acquisition. (B) T_2 results: Image quality with the proposed approach is comparable to 2D bSSFP T_2 mapping and results in similar T_2 values. Spatial variability is reduced by averaging contiguous slices to same slice thickness as for the 2D acquisition

in the left ventricular septum with the proposed joint T_1/T_2 mapping technique (resolution 2 mm isotropic) for both T_1 ($P < .005$) and T_2 quantification ($P < .05$) ($T_{1\,\mathrm{jointT1/T2}}$ variability = 54.7 ± 5.5 ms and $T_{2\,\mathrm{jointT1/T2}}$ variability = 3.9 ± 0.8 ms) with respect to MOLLI (resolution = 1.6 × 1.6 × 8 mm) and T_2-prepared bSSFP T_2 mapping (resolution = 1.8 × 1.8 × 8 mm) that showed, respectively, a variability of $T_{1\mathrm{MOLLI}}$ variability = 41.3 ± 10.5 ms and $T_{2\mathrm{bSSFP}}$ variability = 3.1 ± 0.9 ms.

Comparison with standard 2D mapping techniques was also carried out with respect to mean T_1 and T_2 and COV for each segment of the AHA segment model; results are shown in Supporting Information Figure S7. The proposed technique overestimated the T_1 values in each segment of the left ventricle compared to MOLLI, whereas good agreement in T_2 quantification was found between the T_2-prepared bSSFP T_2 mapping sequence and the proposed 3D joint T_1/T_2 mapping approach. Additionally, higher COVs for both T_1 and T_2 maps were obtained with the proposed technique, although a reduction of COV was observed by reconstructing the maps to the same slice thickness as for the 2D acquisitions.

4 | DISCUSSION

In this work, we proposed a free-breathing motion-compensated sequence for simultaneous acquisition of isotropic-resolution coregistered 3D T_1 and T_2 maps and complementary 3D CMRA and 3D fat volumes in a total scan time of ~9 min.

The proposed approach is based on the acquisition of four 4x accelerated interleaved Dixon GRE datasets acquired with different preparation pulses. The proposed framework is similar to the approach used in Ref. 23 for bSSFP T_2 mapping and anatomical visualization; however, a modification of the sequence design and readout was necessary to guarantee sufficient T_1 and T_2 encoding to provide accurate and precise joint T_1 and T_2 maps. EPG simulations were carried out to assess the capability of the proposed sequence to identify and differentiate T_1 and T_2 pairs corresponding to healthy myocardium, diseased myocardium, and blood. Landscape graph corresponding to the chosen sequence design showed a higher LSE variation around the selected T_1/T_2 pairs and thus a narrower minimum compared to other configurations

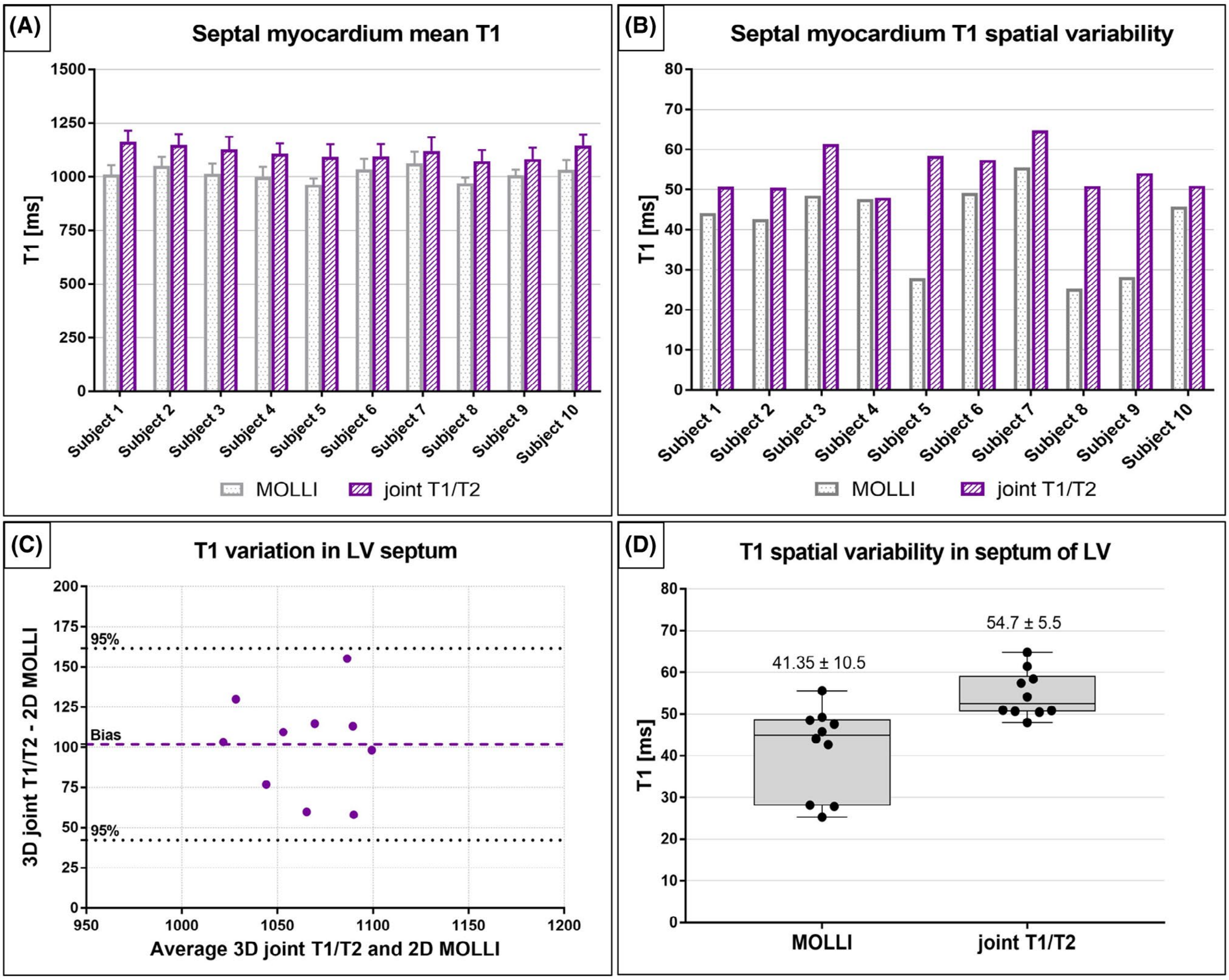

FIGURE 9 Quantitative T_1 results: Measurements were performed in a ROI in the septum of the LV. (A) Comparison of mean T_1s measured for each acquired healthy subject. A T_1 overestimation is observed in comparison to MOLLI acquisition. (B) A higher T_1 spatial variability is obtained with the joint T_1/T_2 mapping sequence for each acquired subject in the septum. (C) Bland Altman analysis between the proposed approach and MOLLI acquisition shows a bias of $T_1 = 101.8$ ms, although T_1 values were within the confidence intervals. (D) Averaged spatial variability across all subjects. ROI, region of interest

(with similar scan time). These findings suggest that the proposed sequence configuration should be able to accurately match the correct T_1/T_2 values for a particular signal evolution in the presence of noise. Furthermore, the Dixon encoded acquisition allowed separation of the fat signal that otherwise could generate motion-related aliasing artefacts in the water images and consequently in the T_1 and T_2 maps (Supporting Information Figure S5) and permitted to boost the SNR of the acquired water volumes. A possible extension of the proposed technique could include a 3-point Dixon acquisition and a more sophisticated water/fat separation algorithm to enable fat quantification and partial volume correction as proposed in Ref. 50.

The proposed 3D joint T_1/T_2 sequence addresses some of the limitations of 2D clinical T_1 and T_2 maps, such as limited coverage and possible misalignment between different scans (T_1 and T_2 maps and anatomical images). The 3D acquisition enabled whole-heart coverage of the myocardium with good uniformity in T_1 and T_2 quantification ($T_1 = 1073 \pm 102$ ms and $T_2 = 42.6 \pm 7.3$ ms for 1 representative subject), although a T_1 underestimation in the lateral portion of the left ventricle was observed for the acquired healthy subjects. Similar underestimation has been reported in previous studies[16,30] and may be caused by residual motion and/or field inhomogeneities.

The isotropic nature of the acquisition permitted reformat of the coregistered T_1/T_2 maps, bright-blood volume, and fat volume in different orientations such as short-axis or 2-chamber or 4-chamber views, maintaining good image quality and clinically feasible scan time in comparison to other recently proposed 3D T_1 and/or T_2 mapping approaches in which a compromise between non-isotropic resolution[16,17,19,29,30]

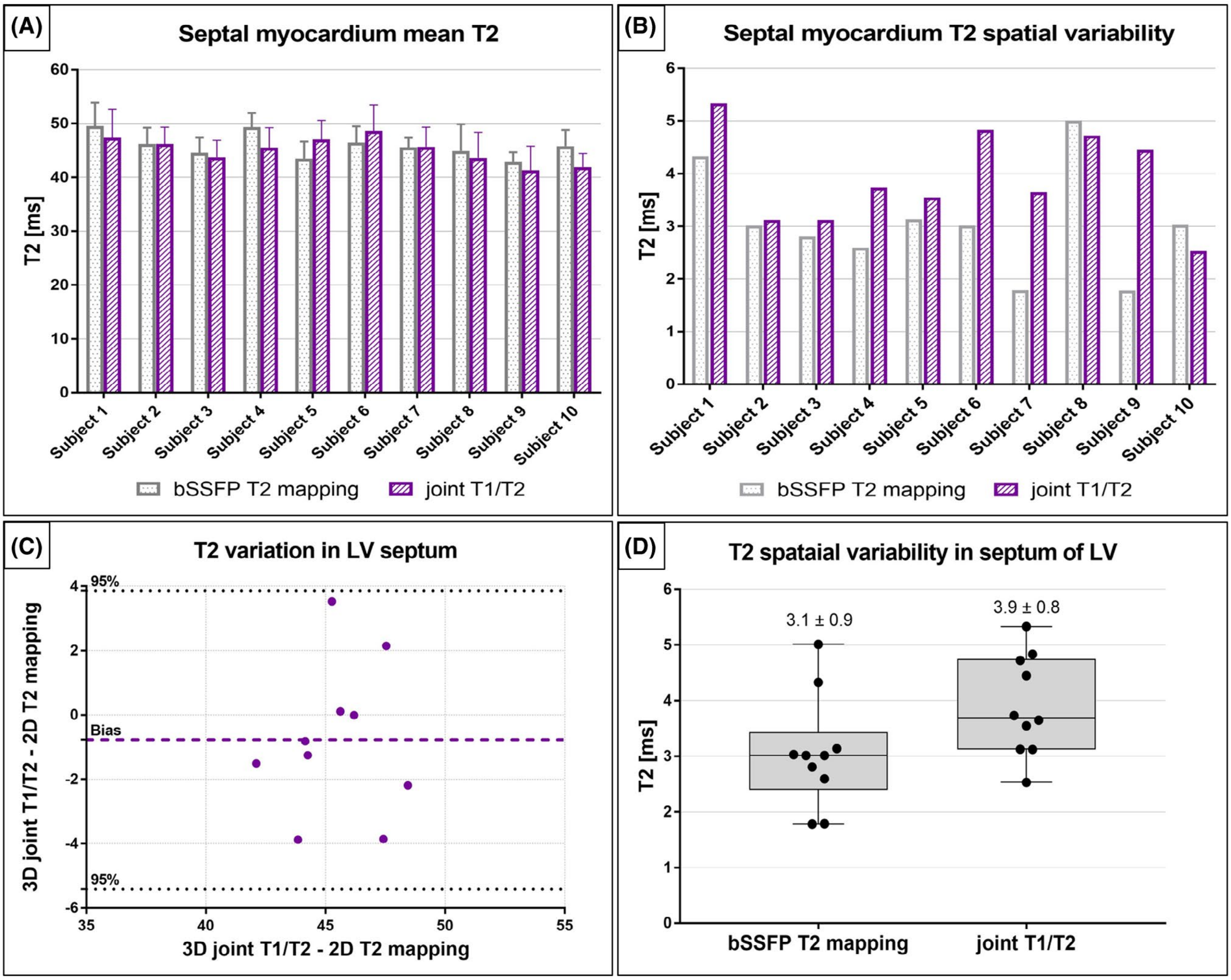

FIGURE 10 Quantitative T_2 results: the measurements were performed in a ROI in the septum. (A) With the proposed approach similar T_2 quantification was obtained in comparison with 2D bSSFP T_2 mapping. A small bias of $T_2 = -0.77$ ms was observed (C). (B and D) Higher spatial variability was observed with the proposed approach

and long scan time[24] had to be made. A recently proposed free-running simultaneous T_1 and T_2 mapping technique enabled the acquisition of coregistered isotropic T_1 and T_2 maps in a clinically feasible scan time[51]; however, long reconstruction time may limit the clinical translation of this technique. In comparison to the latter approach, the method proposed here provides additional cardiac anatomy water and fat images.

The proposed technique showed good agreement with high linear correlation in T_1 and T_2 quantification compared to spin echo references on a standardized phantom. An overestimation and underestimation of long T_1 and T_2, respectively, corresponding to blood vials were observed; however, a similar behavior was obtained with the 2D clinical MOLLI T_1 mapping and bSSFP T_2 mapping techniques. Both T_1 and T_2 over- and underestimation may be due to insufficient T_1 and T_2 encoding of long T_1 and T_2 values; indeed, only 4 points are sampled along the T_1 recovery curve (without acquisition of a fully recovered magnetization image), whereas the longest T_2-prep pulse used in the proposed approach was 50 ms and thus may be too short for encoding for the long T_2 species. T_1 and T_2 variability of <6% and <4% were observed for short T_1/T_2 pairs for HRs ranging between 40 and 120 bpm, whereas higher variability (~10%) were observed for long T_1 and T_2 pairs. A high HR may not allow sufficient time for magnetization recovery in between 2 interleaved acquisitions (especially for long T_1/T_2 values) and could affect the precision of the acquired T_1 and T_2 maps. Although dependency on HR could introduce a bias in T_1 and T_2 quantification, the proposed sequence was able to differentiate between different T_1/T_2 phantom values. Phantom experiments were also performed to evaluate the T_1 and T_2 quantification dependency on the acceleration factor. A small variability of ~3% was observed for acceleration factors ranging between 1 and 4; thus, the chosen 4x accelerated acquisition should not have major effect on the T_1 and T_2 quantification accuracy.

The proposed approach was compared invivo to 2D clinical T_1 and T_2 maps. A T_1 overestimation (T_1 bias = 101.8 ms) was observed in the septum of the left ventricle with respect to MOLLI acquisition; however, T_1 quantified with the proposed sequence was in good agreement with literature values (T_{1myoc} = 1100 ms, mean $T1_{jointT1/T2}$ = 1116 ± 30.5 ms); thus, the known MOLLI T_1 underestimation[52] may contribute to the bias observed. A small bias of T_2 = −0.77 ms was observed with respect to bSSFP T_2 mapping sequence. Higher spatial variability for both T_1 and T_2 in the septum of the left ventricle was found with the proposed approach. Similar findings were observed for the mean T_1 and T_2 values in bull's eye plots. A T_1 overestimation was observed in each of the 16 segments compared to MOLLI (known to underestimate T_1 values[52]), whereas similar T_2 values were obtained compared to standard 2D bSSFP T_2 mapping. The coefficient of variation for each segment was used as metric for spatial variability. Higher COVs for both T_1 and T_2 were obtained with the joint T_1/T_2 sequence. However, the higher spatial variability obtained with the proposed approach may be not only generated by the different sequence but also due to different imaging parameters including spatial resolution. The effect of reconstructing the matched T_1 and T_2 maps to a lower spatial resolution (slice thickness 8 mm) was investigated in AHA 16-segments model. Averaging contiguous slices led to an increased SNR and thus to T_1 and T_2 maps with lower spatial variabilities, whereas no effect was observed on mean T_1 and T_2 values.

A potential limitation of the proposed work is sensitivity to arrhythmia, especially in patients with high or variable HRs. The expected steady-state signal would be affected by arrhythmic heart beats, leading to potential T_1 and T_2 under- or overestimations. A phantom experiment was carried out to assess the effect of a variable HR during the data acquisition; and results are shown in Supporting Information Figure S3. The proposed approach was in good agreement with inversion spin echo and spin echo measurements for T_1 values < 1200 ms and T_2 values < 100 ms; however, a T_2 elevation and T_1 underestimation for long T_1 values was observed, suggesting that highly irregular cardiac rhythms could impair T_1 and T_2 quantification for long T_1 and T_2 values. Integration of arrhythmia rejection in the proposed framework could avoid T_1 and T_2 mismatching. However, the rejection of arrhythmic heartbeats could further increase the undersampling of the data, thus compromising image quality, or increase the total acquisition time. Investigation of retrospective or prospective arrhythmia rejection techniques will be investigated in future studies.

Another limitation of the proposed approach is the assumption of respiratory motion as pure translational superoinferior and left–right displacements. Anteroposterior translational motion and rotational and nonrigid motion of the heart are not considered in the motion correction framework; thus, residual motion could affect the T_1 and T_2 maps in terms of accuracy and spatial variability. More sophisticated nonrigid motion-correction techniques will be incorporated in the reconstruction in the future.[53]

The performance of the proposed approach will be evaluated in patients with both arrhythmic HR and complex respiratory motion in future studies. Furthermore, the suitability of applying the proposed sequence in both pre- and postcontrast to obtain extra cellular volume maps will be investigated.

5 | CONCLUSION

We propose a free-breathing accelerated and motion-corrected 3D joint T_1/T_2 sequence that allows the acquisition of isotropic T_1 and T_2 maps and complementary coregistered bright-blood and fat volumes in a total scan time of ~9 min. The proposed technique showed promising results in terms of T_1 and T_2 quantification compared to standard 2D T_1 and T_2 mapping techniques in phantom acquisitions and in vivo on 10 healthy subjects. Future work will include the acquisition of patients to investigate the capability of the proposed approach to identify T_1 and T_2 elevation associated with cardiovascular diseases.

ACKNOWLEDGMENT
This work was supported by the following: The Engineering and Physical Sciences Research Council (EPSRC) (grants EP/P032311/1, EP/P001009/1, and EP/P007619/1); The British Heart Foundation (BHF) program (grant RG/20/1/34802); King's BHF Centre for Research Excellence (grant RE/18/2/34213); Wellcome EPSRC Centre for Medical Engineering (NS/A000049/1); the Department of Health via the National Institute for Health Research (NIHR) Cardiovascular Health Technology Cooperative (HTC) and comprehensive Biomedical Research Centre awarded to Guy's & St Thomas; the National Health Service (NHS) Foundation Trust in partnership with King's College London; and King's College Hospital NHS Foundation Trust.

CONFLICT OF INTEREST
MR Research Collaborations, Siemens Healthcare Limited, Frimley, United Kingdom.

ORCID
Giorgia Milotta https://orcid.org/0000-0002-3403-3754
Aurelien Bustin https://orcid.org/0000-0002-2845-8617
Olivier Jaubert https://orcid.org/0000-0002-7854-4150

REFERENCES
1. Captur G, Manisty C, Moon JC. Cardiac MRI evaluation of myocardial disease. *Heart*. 2016;102:1429-1435.

2. Salerno M, Kramer CM. Advances in parametric mapping with CMR imaging. *JACC Cardiovasc Imaging*. 2013;6:806-822.
3. Messroghli DR, Walters K, Plein S, et al. Myocardial T1 mapping: Application to patients with acute and chronic myocardial infarction. *Magn Reson Med*. 2007;58:34-40.
4. Puntmann VO, Voigt T, Chen Z, et al. Native T1 mapping in differentiation of normal myocardium from diffuse disease in hypertrophic and dilated cardiomyopathy. *JACC Cardiovasc Imaging*. 2013;6:475-484.
5. Bull S, White SK, Piechnik SK, et al. Human non-contrast T1 values and correlation with histology in diffuse fibrosis. *Heart*. 2013;99:932-937.
6. van Heeswijk RB, Feliciano H, Bongard C, et al. Free-breathing 3 T magnetic resonance T2-mapping of the heart. *JACC Cardiovasc Imaging*. 2012;5:1231-1239.
7. Wassmuth R, Schulz-Menger J. T2-mapping—Clinical experience. *Curr Cardiovasc Imaging Rep*. 2014;7:https://doi.org/10.1007/s12410-013-9251-z.
8. Usman AA, Kirsi T, Marie W, et al. Cardiac magnetic resonance T2 mapping in the monitoring and follow-up of acute cardiac transplant rejection. *Circ Cardiovasc Imaging*. 2012;5:782-790.
9. Messroghli DR, Radjenovic A, Kozerke S, Higgins DM, Sivananthan MU, Ridgway JP. Modified look-locker inversion recovery (MOLLI) for high-resolution T1 mapping of the heart. *Magn Reson Med*. 2004;52:141-146.
10. Piechnik SK, Ferreira VM, Dall'Armellina E, et al. Shortened Modified Look-Locker Inversion recovery (ShMOLLI) for clinical myocardial T1-mapping at 1.5 and 3T within a 9 heartbeat breathhold. *J Cardiovasc Magn Reson*. 2010;12:69.
11. Chow K, Flewitt JA, Green JD, Pagano JJ, Friedrich MG, Thompson RB. Saturation recovery single-shot acquisition (SASHA) for myocardial T1 mapping. *Magn Reson Med*. 2014;71:2082-2095.
12. Montant P, Sigovan M, Revel D, Douek P. MR imaging assessment of myocardial edema with T2 mapping. *Diagn Interv Imaging*. 2015;96:885-890.
13. Giri S, Chung YC, Merchant A, et al. T2 quantification for improved detection of myocardial edema. *J Cardiovasc Magn Reson*. 2009;11:56.
14. Weingärtner S, Akçakaya M, Roujol S, et al. Free-breathing post-contrast three-dimensional T1 mapping: Volumetric assessment of myocardial T1 values. *Magn Reson Med*. 2015;73:214-222.
15. Hu C, Sinusas AJ, Huber S, et al. T1-refBlochi: High resolution 3D post-contrast T1 myocardial mapping based on a single 3D late gadolinium enhancement volume, Bloch equations, and a reference T1. *J Cardiovasc Magn Reson*. 2017;19:63.
16. Nordio G, Henningsson M, Chiribiri A, Villa ADM, Schneider T, Botnar RM. 3D myocardial T 1 mapping using saturation recovery. *J Magn Reson Imaging*. 2017;46:218-227.
17. Guo R, Chen Z, Wang Y, Herzka DA, Luo J, Ding H. Three-dimensional free breathing whole heart cardiovascular magnetic resonance T(1) mapping at 3 T. *J Cardiovasc Magn Reson*. 2018;20:64.
18. Nordio G, Schneider T, Cruz G, et al. Whole-heart T1 mapping using a 2D fat image navigator for respiratory motion compensation. *Magn Reson Med*. 2020;83:178-187.
19. Ding H, Fernandez-de-Manuel L, Schär M, et al. Three-dimensional whole-heart T2 mapping at 3T. *Magn Reson Med*. 2015;74:803-816.
20. Yang H-J, Sharif B, Pang J, et al. Free-breathing, motion-corrected, highly efficient whole heart T2 mapping at 3T with hybrid radial-cartesian trajectory. *Magn Reson Med*. 2016;75:126-136.
21. van Heeswijk RB, Piccini D, Feliciano H, Hullin R, Schwitter J, Stuber M. Self-navigated isotropic three-dimensional cardiac T2 mapping. *Magn Reson Med*. 2015;73:1549-1554.
22. Bustin A, Milotta G, Ismail TF, Neji R, Botnar RM, Prieto C. Accelerated free-breathing whole-heart 3D T2 mapping with high isotropic resolution. *Magn Reson Med*. 2020;83:988-1002.
23. Milotta G, Ginami G, Bustin A, Neji R, Prieto C, Botnar RM. 3D Whole-heart free-breathing qBOOST-T2 mapping. *Magn Reson Med*. 2020;83:1673-1687.
24. van Heeswijk RB, Piccini D, Tozzi P, et al. Three-dimensional self-navigated T2 mapping for the detection of acute cellular rejection after orthotopic heart transplantation. *Transplant Direct*. 2017;3:e149.
25. Messroghli DR, Moon JC, Ferreira VM, et al. Clinical recommendations for cardiovascular magnetic resonance mapping of T1, T2, T2* and extracellular volume: A consensus statement by the Society for Cardiovascular Magnetic Resonance (SCMR) endorsed by the European Association for Cardiovascular Imaging (EACVI). *J Cardiovasc Magn Reson*. 2017;19:75.
26. Chandler AG, Pinder RJ, Netsch T, et al. Correction of misaligned slices in multi-slice cardiovascular magnetic resonance using slice-to-volume registration. *J Cardiovasc Magn Reson*. 2008;10:13.
27. Santini F, Kawel-Boehm N, Greiser A, Bremerich J, Bieri O. Simultaneous T1 and T2 quantification of the myocardium using cardiac balanced-SSFP inversion recovery with interleaved sampling acquisition (CABIRIA). *Magn Reson Med*. 2015;74:365-371.
28. Akçakaya M, Weingärtner S, Basha TA, Roujol S, Bellm S, Nezafat R. Joint myocardial T1 and T2 mapping using a combination of saturation recovery and T 2 -preparation. *Magn Reson Med*. 2016;76:888-896.
29. Kvernby S, Warntjes MJB, Haraldsson H, Carlhäll C-J, Engvall J, Ebbers T. Simultaneous three-dimensional myocardial T1 and T2 mapping in one breath hold with 3D-QALAS. *J Cardiovasc Magn Reson*. 2014;16:102.
30. Guo R, Chen Z, Herzka DA, Luo J, Ding H. A three-dimensional free-breathing sequence for simultaneous myocardial T1 and T2 mapping. *Magn Reson Med*. 2019;81:1031-1043.
31. Hamilton JI, Jiang Y, Ma D, et al. Cardiac MR fingerprinting for T1 and T2 mapping in four heartbeats. *J Cardiovasc Magn Reson*. 2016;18:W1.
32. Börnert P, Koken P, Nehrke K, Eggers H, Ostendorf P. Water/fat-resolved whole-heart Dixon coronary MRA: An initial comparison. *Magn Reson Med*. 2013;71:156-163.
33. Kellman P, Hernando D, Shah S, et al. Multiecho Dixon fat and water separation method for detecting fibrofatty infiltration in the myocardium. *Magn Reson Med*. 2009;61:215-221.
34. Kellman P, Hernando D, Arai AE. Myocardial fat imaging. *Curr Cardiovasc Imaging Rep*. 2010;3:83-91.
35. Dey D, Nakazato R, Li D, Berman DS. Epicardial and thoracic fat—Noninvasive measurement and clinical implications. *Cardiovasc Diagnosis Ther*. 2012;2:85-93.
36. Prieto C, Doneva M, Usman M, et al. Highly efficient respiratory motion compensated free-breathing coronary MRA using golden-step Cartesian acquisition. *J Magn Reson Imaging*. 2014;41:738-746.
37. Bustin A, Ginami G, Cruz G, et al. Five-minute whole-heart coronary MRA with sub-millimeter isotropic resolution, 100%

respiratory scan efficiency, and 3D-PROST reconstruction. *Magn Reson Med*. 2019;81:102-115.
38. Henningsson M, Koken P, Stehning C, Razavi R, Prieto C, Botnar RM. Whole-heart coronary MR angiography with 2D self-navigated image reconstruction. *Magn Reson Med*. 2012;67:437-445.
39. Kosiński W, Michalak P, Gut P. Robust image registration based on mutual information measure. *J Signal Inf Process*. 2012;3:175-178.
40. Bracewell RN, Chang K, Jha AK, Wang Y. Affine theorem for two-dimensional Fourier transform. *Electron Lett*. 1993;29:304.
41. Bustin A, Lima da Cruz G, Jaubert O, Lopez K, Botnar RM, Prieto C. High-dimensionality undersampled patch-based reconstruction (HD-PROST) for accelerated multi-contrast MRI. *Magn Reson Med*. 2019;81:3705-3719.
42. Liu J, Peters DC, Drangova M. Method of B0 mapping with magnitude-based correction for bipolar two-point Dixon cardiac MRI. *Magn Reson Med*. 2016;78:1862-1869.
43. Weigel M. Extended phase graphs: Dephasing, RF pulses, and echoes—Pure and simple. *J Magn Reson Imaging*. 2015;41:266-295.
44. Hamilton JI, Jiang Y, Chen Y, et al. MR fingerprinting for rapid quantification of myocardial T1, T2, and proton spin density. *Magn Reson Med*. 2017;77:1446-1458.
45. Captur G, Gatehouse P, Keenan KE, et al. A medical device-grade T1 and ECV phantom for global T1 mapping quality assurance—The T1 mapping and ECV standardization in cardiovascular magnetic resonance (T1MES) program. *J Cardiovasc Magn Reson*. 2016;18:58.
46. Aletras AH, Kellman P, Derbyshire JA, Arai AE. ACUT2E TSE-SSFP: A hybrid method for T2-weighted imaging of edema in the heart. *Magn Reson Med*. 2008;59:229-235.
47. Kellman P, Arai AE, McVeigh ER, Aletras AH. Phase-sensitive inversion recovery for detecting myocardial infarction using gadolinium-delayed hyperenhancement. *Magn Reson Med*. 2002;47:372-383.
48. Gómez PA, Molina-Romero M, Buonincontri G, Menzel MI, Menze BH. Designing contrasts for rapid, simultaneous parameter quantification and flow visualization with quantitative transient-state imaging. *Sci Rep*. 2019;9:8468.
49. Atlas SW, Grossman RI, Hackney DB, Goldberg HI, Bilaniuk LT, Zimmerman RA. STIR MR imaging of the orbit. *Am J Roentgenol*. 1988;151:1025-1030.
50. Jaubert O, Cruz G, Bustin A, et al. Water/fat Dixon cardiac magnetic resonance fingerprinting. *Magn Reson Med*. 2020;83:2107-2123.
51. Qi H, Bustin A, Cruz G, et al. Free-running simultaneous myocardial T1/T2 mapping and cine imaging with 3D whole-heart coverage and isotropic spatial resolution. *Magn Reson Imaging*. 2019;63:159-169.
52. Kellman P, Hansen MS. T1-mapping in the heart: Accuracy and precision. *J Cardiovasc Magn Reson*. 2014;16:2.
53. Correia T, Cruz G, Schneider T, Botnar RM, Prieto C. Technical note: Accelerated nonrigid motion-compensated isotropic 3D coronary MR angiography. *Med Phys*. 2017;45:214-222.

SUPPORTING INFORMATION

Additional supporting information may be found online in the Supporting Information section.

FIGURE S1 EPG simulations results obtained by plotting the landscape graph of three different sequence configurations for three different tissues (healthy myocardium, diseased myocardium and blood). T_1 and T_2 encoding capability are represented by the narrowness of the minimum identified by the LSE. Similar T_2 encoding is obtained among the three different sequence designs. The GRE readout with FA = 15 degrees adopted in the second configuration increased the T_1 encoding although it may be not sufficient to discriminate between healthy and diseased myocardium. In the third configuration (IR / no-prep / no-prep / T_2-prep) a fourth point was used to increase the T_1 encoding, additionally the acquisition flip angle (FA = 8 degrees) was reduced and a dual-echo Dixon readout was in included. Higher T_1 encoding in obtained with the third configuration

FIGURE S2 Comparison between T_1 and T_2 maps obtained with the proposed approach and conventional 2D MOLLI and T_2-prepared bSSFP T_2 mapping in phantom experiment. (A) Good agreement in T_1 quantification was observed for each phantom vial. Higher standard deviation was observed with the proposed technique in comparison to MOLLI, particularly in the vials with high T_1 values. (B) Good agreement and T_2 quantification and similar standard deviation was observed between the proposed technique and conventional 2D T_2 mapping. A higher standard deviation was observed with the proposed approach in the vial corresponding to blood (vial B)

FIGURE S3 Variable heart rates simulated during phantom data acquisition. The heart rate ranged between 60 bpm and 100 bpm with variation applied every ~30 sec. T_1 underestimation of long T_1 vial corresponding to blood is observed with the proposed approach in comparison to inversion spin echo (IRSE) acquisition. A slight T_2 overestimation of short T_2 values is observed with the proposed approach in comparison to spin echo (SE) results

FIGURE S4 Measured signal evolution through the four contrast of each phantom vial and oil bottle in the water volume (top row) and fat volume (bottom row). Good fat/water separation is observed in each acquired contrast. The fat signal is low in the water images consistently across the four acquired contrasts, similarly the water signal evolution through the four datasets of each phantom vial is close to zero in the fat images

FIGURE S5 T_1 and T_2 maps reconstructed with and without water/fat separation step for one representative healthy subject. Pericardial fat is clearly visible in the T_1 and T_2 maps reconstructed without water/fat separation. Although no major differences were observed in the mean septal T_1 and T_2 values obtained with the two approaches ($T_{1no\_W/F}$ = 1138 ± 151 ms, $T_{2no\_W/F}$ = 43 ± 7.2 ms, $T_{1W/F}$ =1076 ± 62 ms and $T_{2W/F}$ = 45 ± 2.6 ms) motion related aliasing artefacts from the fat signal may affect the spatial variability of the quantified T_1 and T_2 values

FIGURE S6 Bull's eye plot and box plot of mean T_1 (A and C) and T_2 (B and D) quantification obtained with the joint T_1/T_2 sequence averaged across all subjects. A T_1 underestimation is observed in the lateral part of the left ventricle; a similar small, non-significant, T_2 underestimation is observed

FIGURE S7 AHA 16-segment bull's eye plot of mean T_1 and T_2 values and coefficient of variation obtained with the proposed sequence and with standard MOLLI and bSSFP T_2 mapping sequences. A T_1 overestimation is observed with the proposed acquisition for each segment, whereas good agreement in mean T_2 quantification is observed. Higher COVs are obtained for both T_1 and T_2 quantified with the proposed approach, although by reconstructing the maps to the same slice thickness as the 2D acquisition the COVs are reduced

TABLE S1 Acquisition parameters of 2D bSSFP T_2 mapping and MOLLI techniques, 3D Dixon CMRA and the proposed joint T_1/T_2. Clinically used imaging parameters were used for the acquisition of the standard T_1 and T_2 maps, whereas matching imaging parameters were adopted for the 3D acquisitions Acquisition parameters of 2D bSSFP T_2 mapping and MOLLI techniques, 3D Dixon CMRA and the proposed joint T_1/T_2. Clinically used imaging parameters were used for the acquisition of the standard T_1 and T_2 maps, whereas matching imaging parameters were adopted for the 3D acquisitions

TABLE S2 Quantification of the EPG simulations results. T_1 and T_2 LSE variation calculated for three sequence configurations and three tissues (healthy myocardium, diseased myocardium and blood). T_1 LSE variation was calculated as the LSE variation for a T_1 ranging between ±100 ms from the selected T_1 (minimum LSE). Similarly, T_2 LSE variation was quantified for T_2 ranging ±15 ms from the selected T_2 value. LSE variations are reported as variation corresponding to "negative T_1 or T_2 variation"—"positive T_1 or T_2 variation". Strong T_1 and T_2 encoding are represented by high T_1 and T_2 LSE variations. The third sequence configuration showed a good trade-off between high T_1 and T_2 encoding

How to cite this article: Milotta G, Bustin A, Jaubert O, Neji R, Prieto C, Botnar RM. 3D whole-heart isotropic-resolution motion-compensated joint T_1/T_2 mapping and water/fat imaging. *Magn Reson Med*. 2020;84:3009–3026. https://doi.org/10.1002/mrm.28330